telecom

MDPI

Article

Unique Dielectric Protection for Microwave and Millimeter-Wave Antenna Applications

Hafiz Usman Tahseen [1,*], Luca Francioso [1], Syed Shah Irfan Hussain [2] and Luca Catarinucci [3]

[1] IMM-CNR, National Research Council of Italy Lecce, 73100 Lecce, Italy; lucanunzio.francioso@cnr.it
[2] Department of Electrical Engineering, University of Engineering and Technology, Lahore 54890, Pakistan; ssirfanhussain@uet.edu.pk
[3] Department of Innovation Engineering, University of Salento, 73100 Lecce, Italy; luca.catarinucci@unisalento.it
* Correspondence: hafizusmantahseen@cnr.it

Abstract

Dielectric covers are generally used to provide external protection to antenna systems by providing electromagnetic transparency. They are utilized in ground applications as well as for protecting airborne, Sat Com, terrestrial and underwater antenna installations. This paper presents a unique and universal design of dielectric sandwich-layered cover that can effectively protect antennas operating in a large frequency band from 1 GHz to 28 GHz, including millimeter-wave and microwave ranges, with minimum insertion loss for various incident angles. The proposed single dielectric cover may give sufficient protection for an entire tower or chimney housing multiple antennas, ranging from first-generation to fifth-generation microwave base-station antennas, as well as other wireless/broadcast antennas in millimeter or lower frequency ranges. In the first step, optimum dielectric constant and thickness of the dielectric cover are calculated numerically through a MATLAB (R2015a) code. In the second step, a floquet port analysis is performed to observe the insertion loss through the transmission coefficient against various frequency band-spectrums in microwave and millimeter-wave ranges for validation of the proposed synthesis. The ANSYS 18.2 HFSS tool is used for the purpose. In the third step, fabrication of the dielectric-layered structure is completed with the optimum design parameters. In the final step, the dielectric package is tested under various fabricated antennas in different frequency ranges.

Keywords: dielectric protection; antenna; dielectric-layered structure

Academic Editor: George Tsoulos

Received: 9 August 2025
Revised: 16 September 2025
Accepted: 26 September 2025
Published: 4 October 2025

Citation: Tahseen, H.U.; Francioso, L.; Hussain, S.S.I.; Catarinucci, L. Unique Dielectric Protection for Microwave and Millimeter-Wave Antenna Applications. *Telecom* **2025**, *6*, 74. https://doi.org/10.3390/telecom6040074

1. Introduction

Radomes mounted on missiles and aircrafts serve to protect antennas from severe external environmental conditions [1]. In addition to efficient mechanical performance like thermal resistance and rigidity, radome covers should not affect the radiation patterns. The coating layers on a radome cover gives protection against high temperatures in high-speed applications [2]. Antennas are mounted on military and commercial aircrafts for airborne applications. Some examples of antenna radome systems are maritime, terrestrial and airborne applications. Low loss is a crucial requirement for any dielectric cover or radome design during antenna operation, allowing for better system applications. Insertion loss also increases due to the internal reflection. Several techniques have been adopted for the electromagnetic performance enhancement of radomes using frequency-selective surfaces, resonant or semi-resonant dielectric involvement, meta-materials, etc. [3–5]. Dielectric materials are also merged in the radome walls for performance enhancement [6]. A radome

with a graded dielectric–inhomogeneous wall is proposed in [7] with a stream-lined nose-cone shape. In [8], an optimum A-sandwich dielectric radome was used for antenna operations in comparison with the C-sandwich and multi-layered wall configurations with minimum insertion loss. A dual-band A-sandwich radome is proposed in [9] for airborne applications. Several techniques are described in [10] for radome design and EM (electromagnetic) analysis. A genetic algorithm is used to optimize an A-sandwich radome in [11]. The particle swarm optimization technique is used along with a 3D tracing method in [12] to optimize transmission loss and BSE (bore-site error) of a dielectric radome. A variable thickness radome is proposed in [13].

In the literature review mentioned above, several dielectric covers with various wall configurations are proposed to ensure a small insertion loss, and they were designed for a specific antenna/band range. The target of this proposed dielectric structure is to give almost the same minimum reflection behavior (insertion loss) to all antennas (either in the microwave frequency range or millimeter-wave range). The ultimate goal is to ensure that the proposed dielectric structure may affect the radiation pattern as minimally as possible, with this effect remaining the same for all of the frequency bands during antenna operations. The ability to give less insertion loss as compared to the previous works and the feasibility of using various frequency bands, i.e., (microwave and mm-wave range) from 1 GHz to 28 GHz, will make it a unique candidate for a universal protective solution for transceiver chimneys and towers.

Firstly, a MATLAB code is developed to calculate an optimum thickness and dielectric constant values for a sandwich structural configuration using Equations (1)–(7) [14]. In the next step, floquet port analysis is performed to observe the insertion loss for various frequency band values with the optimum thickness and dielectric constant of the radome/cover material. Once this synthesis is validated through floquet port analysis, a radome-shaped dielectric cover is simulated to see the antenna gain for various antennas for various frequency bands. Finally, a protective structure is realized and tested with various antennas in different frequency ranges.

The paper is organized as follows: the design of a dielectric-layered structure and EM analysis is given in Section 2. The EM analysis of various antennas (in different frequency ranges) with a dielectric-layered radome/cover is given in Section 3. The fabrication, along with measurements, is given in Section 4. The final summary is in Section 5.

2. Design of Dielectric-Layered Sandwich Structure

Parameters like ray incident angle, material thickness, polarization, dielectric constant and loss tangent have notable effects on ray transmission. For this purpose, Equations (1)–(7) evaluate the effect/behavior of electromagnetic waves at any incident angle and polarization through a dielectric material structure. For the normal ray incident angle, the levels become independent of polarization, but they give various polarization distortions and reflections for angles other than the normal incident angle, i.e., 0–80°. These polarization distortions and reflections may give rise to varying levels of absorption loss, and reflected and transmitted waves. The concept of an equivalent transmission line is adopted as explained in [14], where a dielectric layer/sheet becomes a low-impedance length of line. The number of layers in a sandwich structure results in a conceptual series of such low impedances. Each length of line (layer) is represented by a standard matrix that performs multiplication results for the properties of the multi-layer structure in a single representation. Thus, the final matrix that represents a single layer or a series of layers has the form $\begin{bmatrix} A & B \\ C & D \end{bmatrix}$ [14].

In radome design, the ABCD matrix is a tool used to model mathematically how signals or electromagnetic waves travel through the dielectric layers of a radome. This mechanism is a valuable method that calculates an electromagnetic performance, i.e., reflection and transmission, for multi-layered wall configurations of radome through a transmission line model. By considering each layer stage as a separate matrix, all individual matrices are multiplied to get an overall ABCD matrix that is used for estimating the total reflection and transmission coefficients of radome as a function of angle and frequency. The ABCD matrix is a unitless matrix that shows a transfer function of wave propagation through dielectric layers and describes an input–output relationship.

The overall ABCD matrix characterizing the skin–core–skin can be written as follows [10,14]:

$$\begin{bmatrix} A & B \\ C & D \end{bmatrix} = \begin{bmatrix} A_s & B_s \\ C_s & D_s \end{bmatrix} \begin{bmatrix} A_c & B_c \\ C_c & D_c \end{bmatrix} \begin{bmatrix} A_s & B_s \\ C_s & D_s \end{bmatrix} \tag{1}$$

where the *s* and *c* subscripts refer to the skin and core layers, respectively. So, the reflection R and transmission T coefficients can be calculated using

$$R = \frac{A + B - C - D}{A + B + C + D} \tag{2}$$

$$T = \frac{2}{A + B + C + D} \tag{3}$$

However, the ABCD single-layer matrix is given by

$$\begin{bmatrix} \cos\varphi & j\frac{z}{z_0}\sin\varphi \\ j\frac{z}{z_0}\sin\varphi & \cos\varphi \end{bmatrix} \tag{4}$$

The electric length is

$$\varphi = \frac{2\pi\, d\sqrt{\varepsilon - \sin\theta^2}}{\lambda} \tag{5}$$

where λ is a free-space wave length, d is the layer thickness and θ is the incident angle. For each value of skin thickness, the transmission coefficient changes with the incident angle.

The ratio of the impedance $\frac{z}{z_0}$ (medium to that in free space) is given by

$$\frac{\sqrt{\epsilon - \sin\theta^2}}{\epsilon\cos\theta} \text{ (Parallel)} \tag{6}$$

$$\frac{\cos\theta}{\sqrt{\epsilon - \sin\theta^2}} \text{ (Perpendicular)} \tag{7}$$

Out of the various choices for dielectric wall configurations of radomes, A-sandwich has been the most commonly selected and reliable dielectric-layered protective structure for antennas [5,8,9,11]. In the A-sandwich dielectric-layered package, two dielectric skin layers with relative permittivity ε_s are used to enclose the central core layer with relative permittivity $\varepsilon_c < \varepsilon_s$. This configuration offers a good strength-to-weight ratio and transmission efficiency, even at various incident angles. The dielectric-layered structure can be represented by an equivalent transmission line [14]. Therefore, the multi-layered dielectric package functions as a transmission line with various small lengths. These dielectric layers exhibit different impedances for horizontal and vertical polarizations. The sequence of layers in the A-sandwich dielectric-layered configuration is skin–core–skin.

For a single-layer structure, the most commonly used dielectric materials are from dielectric constants from 1.5 (ground-based foam radome) to 9 (alumina-based missile radome). Resin-glass fiber is the most commonly used material with a dielectric constant

of 4. Typically, a three-layered A-sandwich structure is used with a resin-glass fiber skin (dielectric constant of 4) and honey-comb core material (dielectric constant of 1.15).

With reference to the radome design methodology [14], the authors develop a synthesis to calculate numerically the optimum thickness for skin and core materials with relevant dielectric constant values. For this purpose, a MATLAB code is developed using Equations (1)–(7) to find the optimum skin and core thickness (satisfying perpendicular polarization transmission with various incident angles 0°, 45°, 60° and 80°) by varying dielectric constant values.

In the first step, transmission characteristics are shown for different core materials (with various dielectric constant values) keeping the skin thickness fixed (0.03 thickness-to-wavelength ratio, i.e., 0.957 mm [14]) at 9.4 GHz. The transmitted power is calculated numerically through a MATLAB code as a percentage for the core material by varying the dielectric constant value in steps (dielectric constant = 6, 4, 3 and 1.15) with the fixed-skin dielectric constant and thickness values for the incident angles 0°, 45°, 60° and 80° as shown in Figures 1–4. It can be observed from the results that the transmission is better with a dielectric constant of 1.15 for the incident angles 0°, 45°, 60° and 80° for both of the optimization cases shown in Figure 4. This graph yields an optimum thickness-to-wavelength ratio of 0.304 (for perpendicular polarization). The dielectric cover is to be used for the antennas (designed with perpendicular polarization), so the optimum and ultimate core thickness is 0.304λ, i.e., 9.7 mm. In the second step, the skin dielectric constant value is varied (keeping fixed the optimum core with a 1.15 dielectric constant, 9.7 mm thickness and skin thickness of 0.03λ, i.e., 0.957 mm). It can be observed from Figure 5a–c that the optimum skin dielectric constant is 3.23 with a 0.957 mm thickness. It is clear from Figure 5c that the skin is satisfied with an optimum value of 0.304λ (9.7 mm) core thickness only with a dielectric constant of 3.23 and a fixed thickness of 0.957 mm. In the third step, the code is run each time for one fixed incident angle i.e., (0°, 45°, 60° and 80°) for various dielectric constant values of core material as shown in Figure 6a–d. It can be seen that the transmission remains good throughout the various thickness values for all incident angles at the optimum dielectric constant, i.e., 1.15. This exercise is performed at a central design frequency of 9.4 GHz. To check that the proposed synthesis can be applicable to all frequency spectrums, the code is run for various frequency bands (in microwave and millimeter-wave ranges) with the optimum thickness and dielectric constant values of a dielectric structure as shown in Figure 7. It is clear that the transmission remains the same and is unique throughout the axis when the code is run for various frequency bands with the optimum dielectric design values.

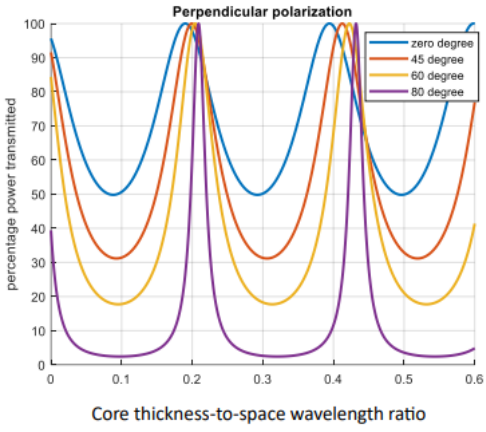

Figure 1. Power transmission with core. Dielectric constant = 6 for the fixed-skin dielectric constant (3.23) and thickness 0.03λ (0.957 mm); for perpendicular polarization.

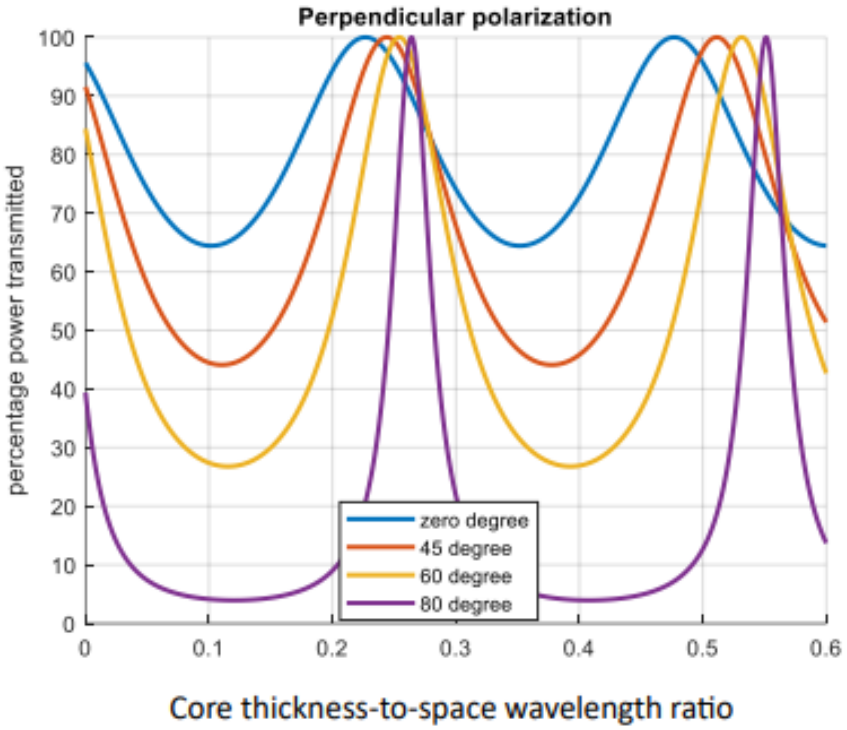

Figure 2. Power transmission with core. Dielectric constant = 4 for the fixed-skin dielectric constant (3.23) and thickness 0.03λ (0.957 mm); for perpendicular polarization.

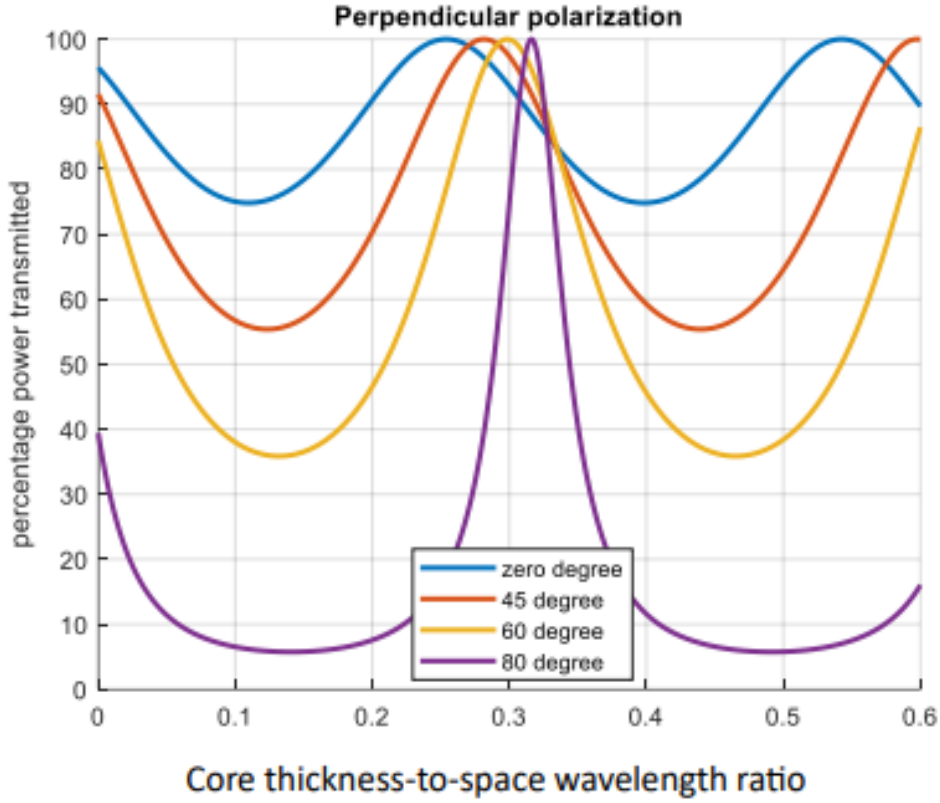

Figure 3. Power transmission with core. Dielectric constant = 3 for the fixed-skin dielectric constant (3.23) and thickness 0.03λ (0.957 mm); for perpendicular polarization.

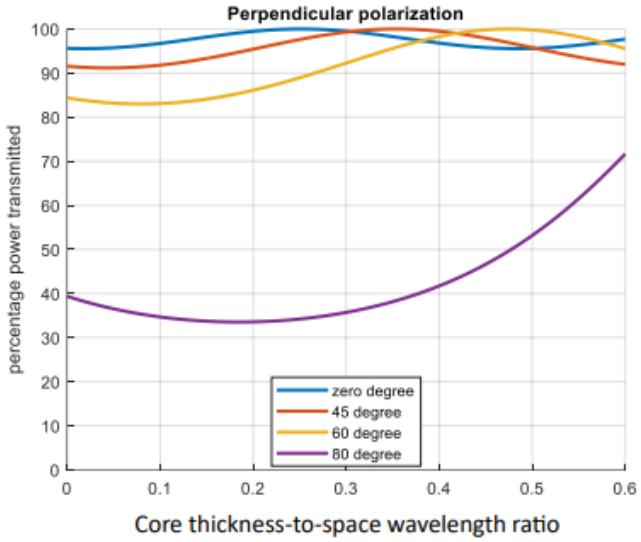

Figure 4. Power transmission with core. Dielectric constant = 1.15 for the fixed-skin dielectric constant (3.23) and thickness 0.03λ (0.957 mm); for perpendicular polarization.

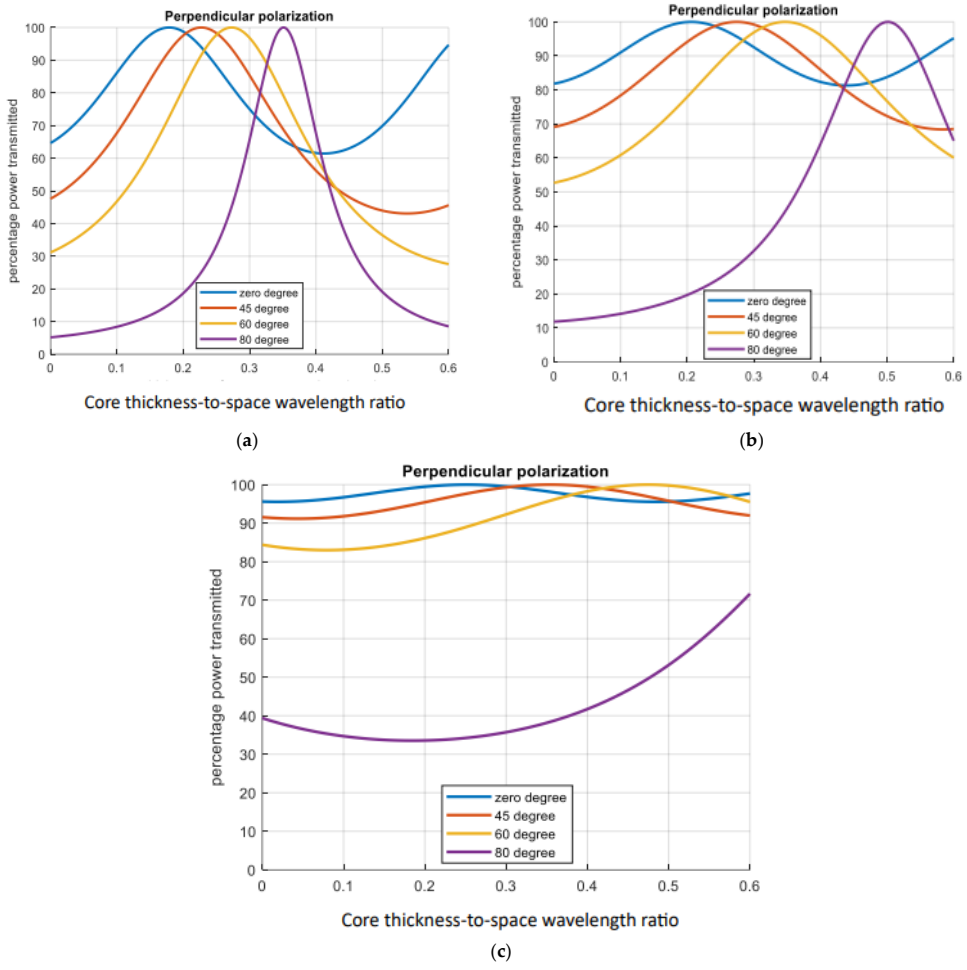

Figure 5. Power transmission by varying skin dielectric constant with fixed core dielectric constant = 1.15 (with 9.7 mm thickness) and fixed skin thickness is 0.03λ (0.957 mm). (**a**) Skin dielectric constant = 9, (**b**) skin dielectric constant = 6 and (**c**) skin dielectric constant = 3.23.

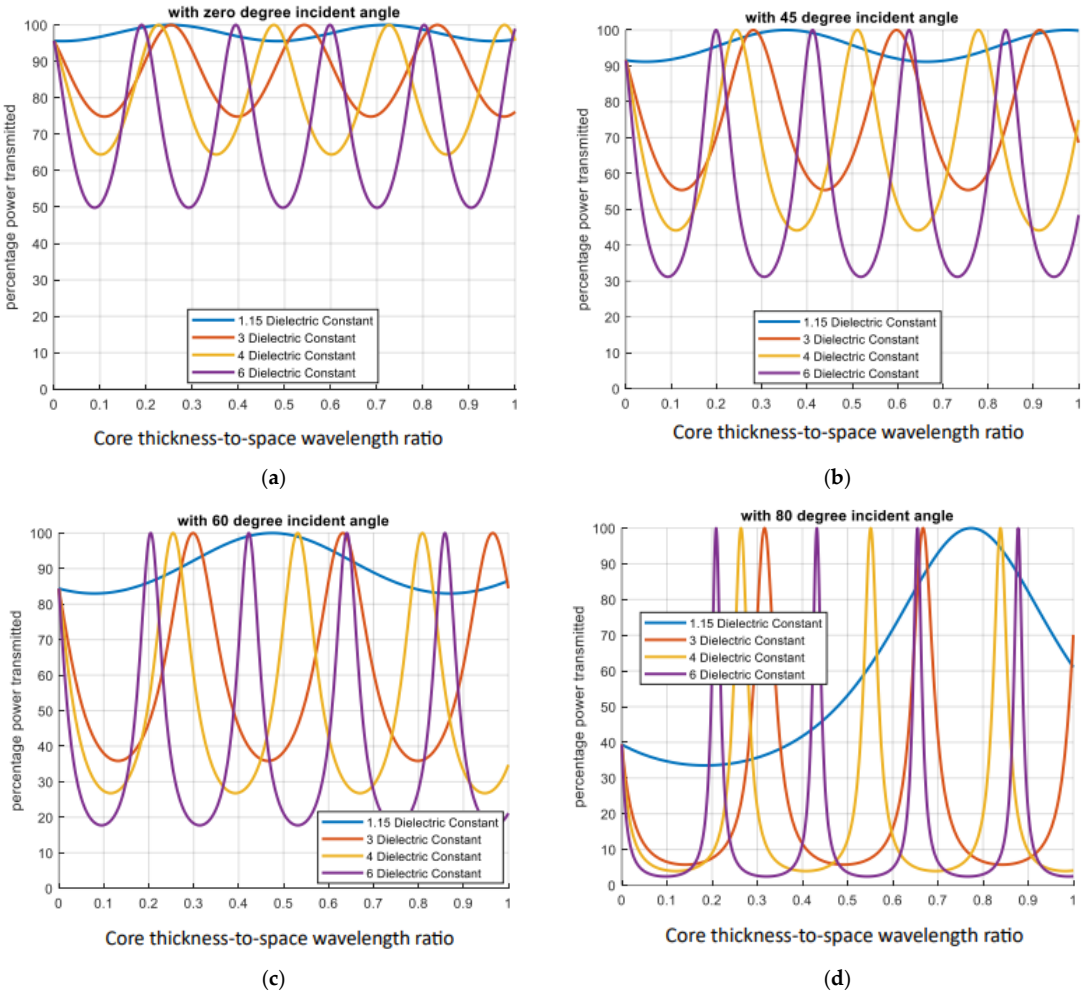

Figure 6. Transmission at fixed incident angle by varying dielectric constant: (**a**) at 0°, (**b**) at 45°, (**c**) at 60° and (**d**) at 80°.

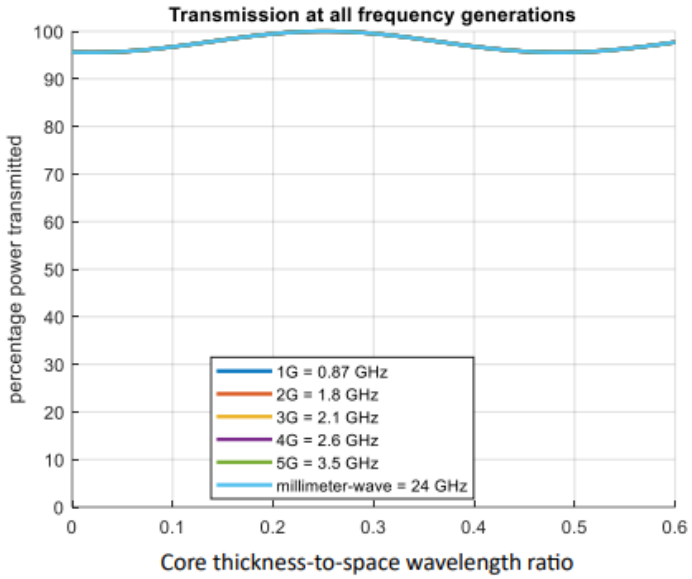

Figure 7. Transmission with the optimum parameter at various frequency bands.

It can be observed from all of the above results that the dielectric material gives its maximum transmission at a specific thickness and dielectric constant value for different incident angles. This optimum point moves forward and is transferred to a greater thickness value as the dielectric constant value is decreased. Furthermore, only the optimum dielectric constant value covers the wide range of thickness bands to give a transmission efficiency near or above 90%, but the rest of the dielectric values give a high transmission efficiency for only one or two specific points with a sharp downfall. It can also be observed that there is a minimum thickness band for the 80° incident angle not only for the optimum case but also for all of other above-graph results. It can be seen from Figure 8 that transmission happened for only one specific and precise thickness point for all of the dielectric values except for the optimum (1.15 dielectric constant, which gives 100% (maximum) at one point but covers a thickness band with a lower percentage. When the code is run for three further increased incident angles, i.e., 85°, 89° and 90°, with this unique behavior of dielectric material, it can be observed that the thickness band becomes narrower and requires a precise and specific thickness but the optimum (1.15 dielectric constant) is moving forward as shown in Figure 9a,b. This behavior is confirmed until the antenna LOS (line of sight) disappears at the 90° angle as shown in Figure 9c.

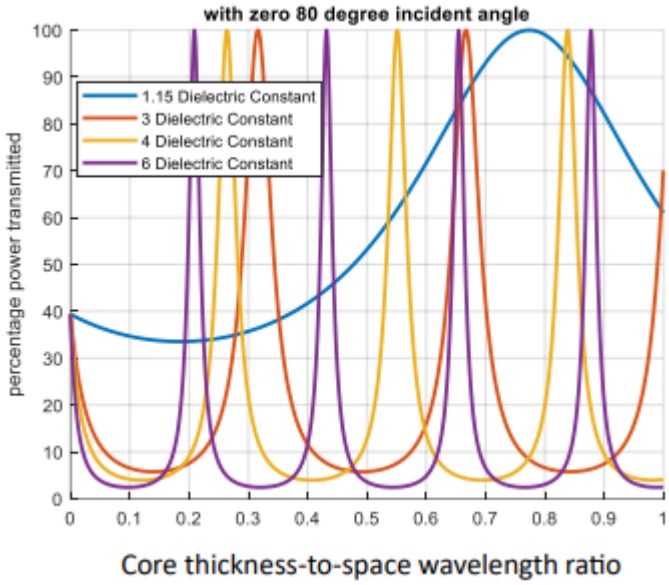

Figure 8. Thickness bands for the transmission at 80° incident angle for various dielectric constant values.

A floquet port analysis is performed with the optimum numerically calculated data for the dielectric core and skin materials for validation of the synthesis through simulation. A unit cell (measuring 60 mm × 60 mm as depicted in Figure 10) is simulated using the ANSYS 18.2 HFSS tool. For this purpose, this unit cell with a sandwich structure incorporates Quartz-polycyanate skin and Rohacell_110WF core materials, with respective thicknesses of 0.957 mm and 9.7 mm and dielectric constant values of 3.23 and 1.15, respectively. The Quartz has a base-material dielectric constant in the range of 3.78 to 4 for the frequency range 1 to 40 GHz. For the proposed structure, an optimized Quart-polycyanate composite is used with a dielectric constant of 3.23, dielectric loss of 0.002 δ, tensile strength of 1.75 GPa and softening point of 1600 °C. The Rohacell_110WF is a high-performance polymethacrylimide foam with a dielectric constant of 1.15, density of 110 kg/m^3, tensile strength of 3.7 MPa, softening point of 350 °C and dielectric loss of 0.0003 δ.

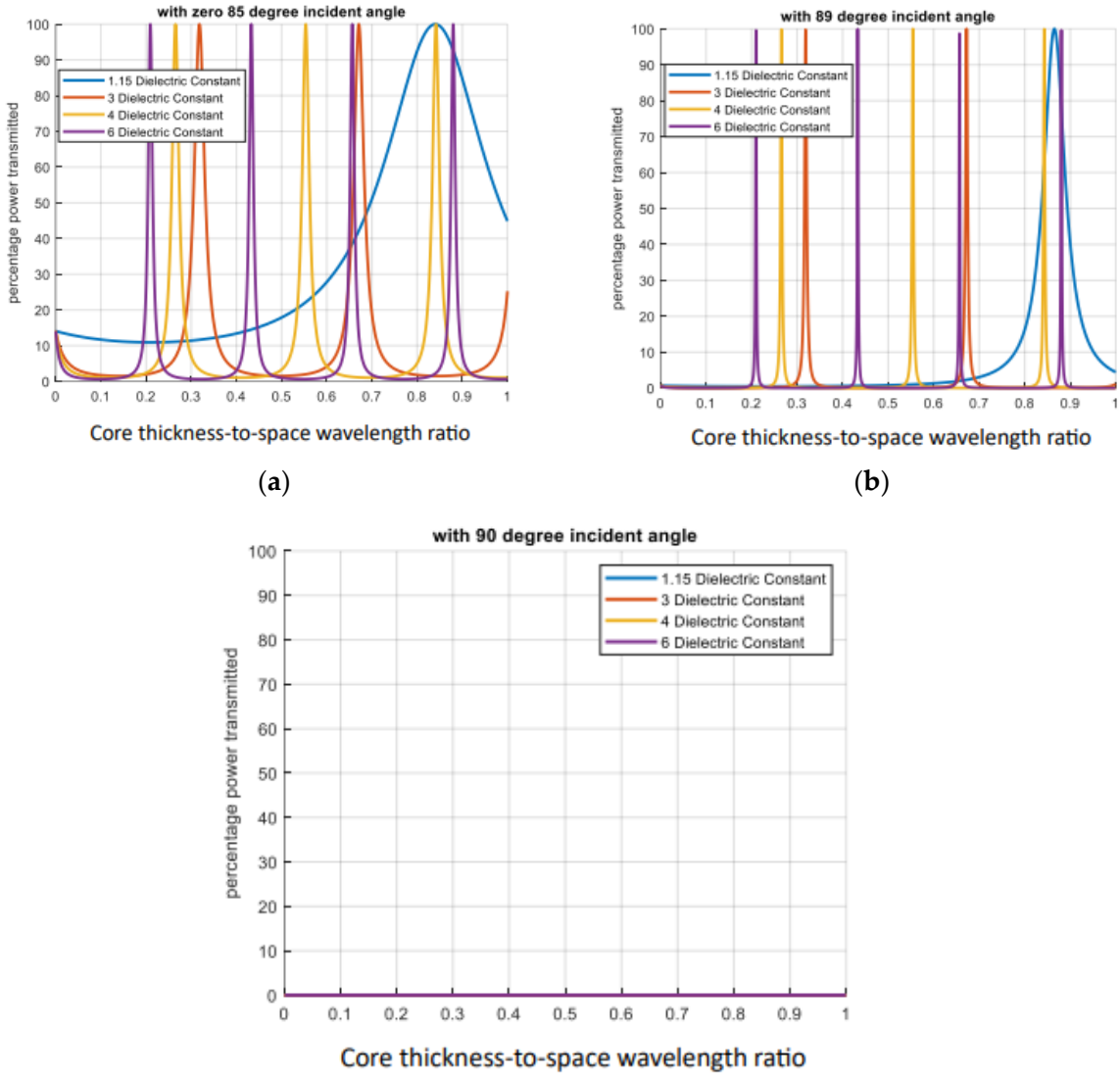

Figure 9. Transmission at extreme positions of LOS (line of sight): (**a**) at 85°, (**b**) 89° and (**c**) 90°.

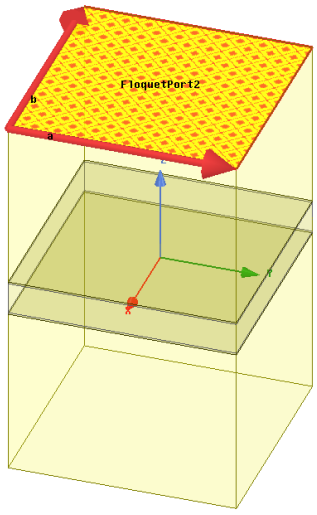

Figure 10. Dielectric A-sandwich unit cell.

The transmission coefficient in Figure 11a shows a comparison for the transmission coefficient of various dielectric-sandwich structures (A-sandwich, C-sandwich and multi-

layered sandwich). It can be observed that all three structures give a good transmission coefficient up to 60° incident angle with a little difference but A-sandwich makes a difference with better coefficient value beyond 60°. In the next step, the same analysis is performed with a selected A-sandwich structure for various randomly selected frequencies in microwave and millimeter-wave ranges at different incident angles as shown in Figure 11b. It can be seen that the dielectric A-sandwich structure with the numerically calculated optimum parameters gives good transmission coefficient for the incident angles 0–80° for each of mentioned frequencies. Hence, an optimum A-sandwich dielectric package is made with the optimum design parameters (flat or radome-shaped).

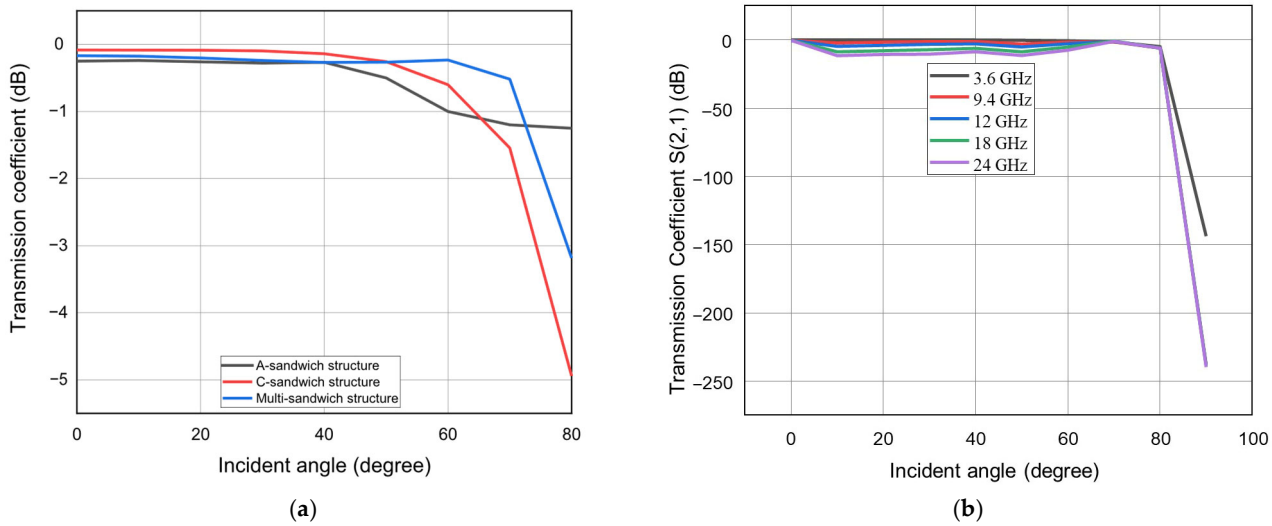

Figure 11. Insertion loss through transmission coefficient with optimum skin and core materials: (**a**) comparison among various structural configurations and (**b**) transmission behavior of selected A-sandwich configuration for various frequency signals.

3. EM Analysis of Antennas with Dielectric-Layered Sandwich Structure

In this section, simulations are performed for various antennas (in microwave and millimeter-wave frequency ranges) under dielectric-layered protective structures (radome-shaped and straight panel). The interest is focused on the effect of dielectric-layered structures on various performance parameters (gain, bandwidth, radiation efficiency and HPBW).

3.1. EM Analysis of Microwave Sub-6 GHz Antennas

A sub-6 GHz 5G antenna shown in Figure 12 is simulated. This antenna covers the frequency bands of 3.6–3.85 GHz, 4.05–4.2 GHz and 4.8–4.95 GHz with S_{11} and S_{22} values below −15 dB. The antenna is tested under both dielectric-layered protective structures (radome and plate) as depicted in Figure 12. The antenna performance parameters (gain, bandwidth, efficiency and HPBW) are observed as shown in Figure 13. The simulated radiation patterns, reflection coefficient and antenna efficiency, with and without the dielectric-layered structures, are given in Figure 13. It is evident that the antenna without dielectric protection exhibits a slightly higher peak gain value of 7 dBi compared to the other cases. Interestingly, even with the introduction of dielectric protective structures, the gain remains consistent at 6.85 dBi. Additionally, the radiation patterns for all three scenarios are remarkably similar, and are characterized by an equal half-power beamwidth (HPBW), i.e., 65° but a slight beam-squint towards the left side. Consequently, the impact of reflections from the dielectric materials are relatively minimal. Similarly, a slight upward shift of S_{11} and the efficiency graph are observed without affecting the gain value and resonance frequency as shown in Figure 13b,c. For the S_{11} parameter, the graph pattern

shifts a little upward for the first two bands due to the dielectric surface reflections. Despite this, the overall efficiency graph follows the same pattern for the frequency sweep within the specified bands, including a little reflection for the dielectric structure scenario as shown in Figure 13c.

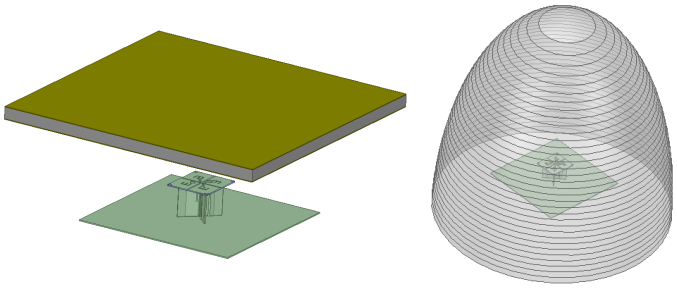

(**a**) (**b**)

Figure 12. 5G antenna under dielectric-layered A-sandwich protective structures: (**a**) antenna under a dielectric-layered A-sandwich straight panel (200 mm × 200 mm) structure and (**b**) antenna under a dielectric-layered A-sandwich radome structure (bottom radius = 160 mm, middle layer radius= 140 mm, top layer radius = 36 mm and height = 320 mm).

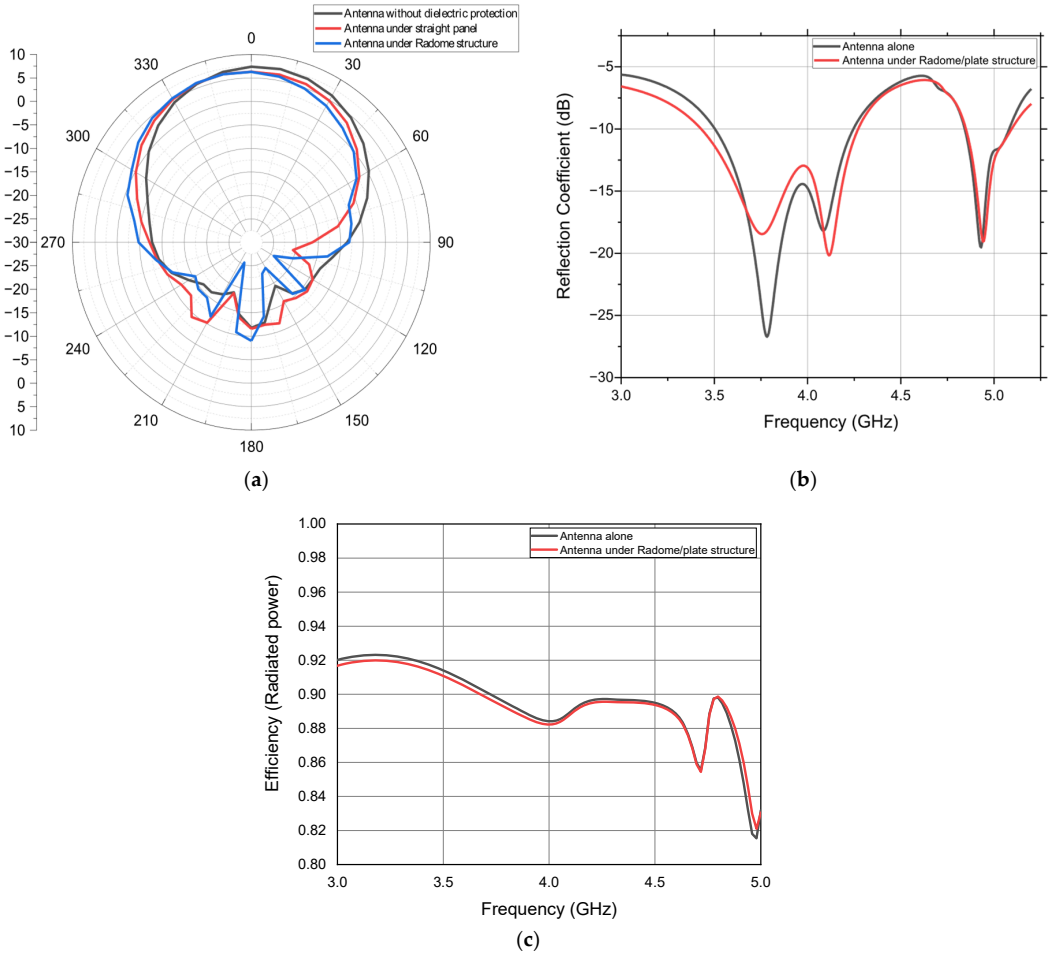

(**a**) (**b**)

(**c**)

Figure 13. Various performance parameters for a microwave 5G antenna with and without dielectric cover: (**a**) antenna radiation patterns, (**b**) antenna S_{11} parameter to show impedance bandwidth and (**c**) radiation efficiency (radiated power).

3.2. EM Analysis of Microwave X-Band Antenna

A WR-90 horn antenna operating in the X-band range, with a design frequency of 9.4 GHz, is simulated under two dielectric structures, as illustrated in Figure 14a,b. The antenna demonstrates a significant impedance bandwidth starting at 9 GHz and beyond. Moreover, the antenna alone achieves a simulated gain of 20.23 dBi at 9.4 GHz, as depicted in Figure 15a. When placed under a dielectric straight panel (measuring 600 mm × 600 mm) and a radome, the antenna exhibits simulated gains of 20.20 dBi and 20 dBi, respectively. It has been observed that directional antennas experience minimal reflection compared to isotropic antennas. Consequently, the impact of the dielectric packaging on the antenna pattern is minimal. Moreover, the S_{11} parameter and radiation efficiency graphs are also given in Figure 15b,c. A small variable reflection is observed through the frequency sweep within the specified band that does not impact on the peak gain value at resonance frequency. The impact of much of the reflection is observed on the side lobes and back lobe of the antenna gain (radiation) patterns as shown in Figures 13a and 15a.

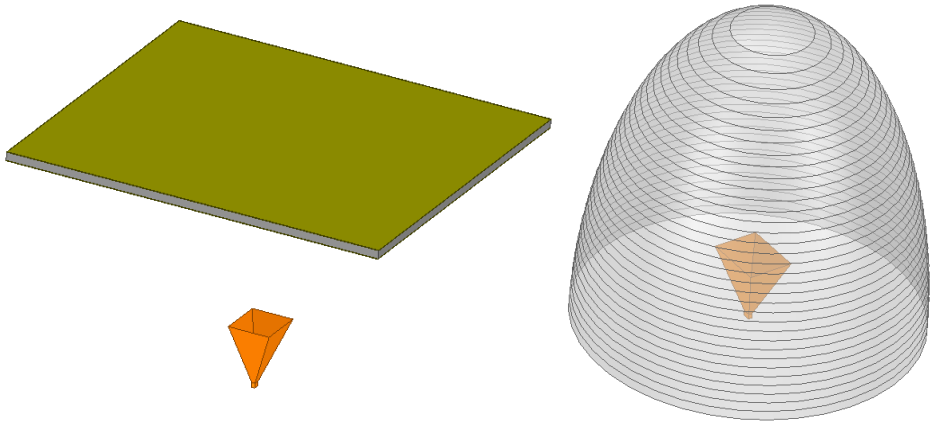

(**a**) (**b**)

Figure 14. X-band horn antenna under dielectric-layered protective structures: (**a**) antenna under a dielectric-layered straight panel structure, (**b**) antenna under a dielectric-layered radome structure (bottom radius = 160 mm, middle layer radius = 140 mm, top layer radius = 36 mm and height = 350 mm.

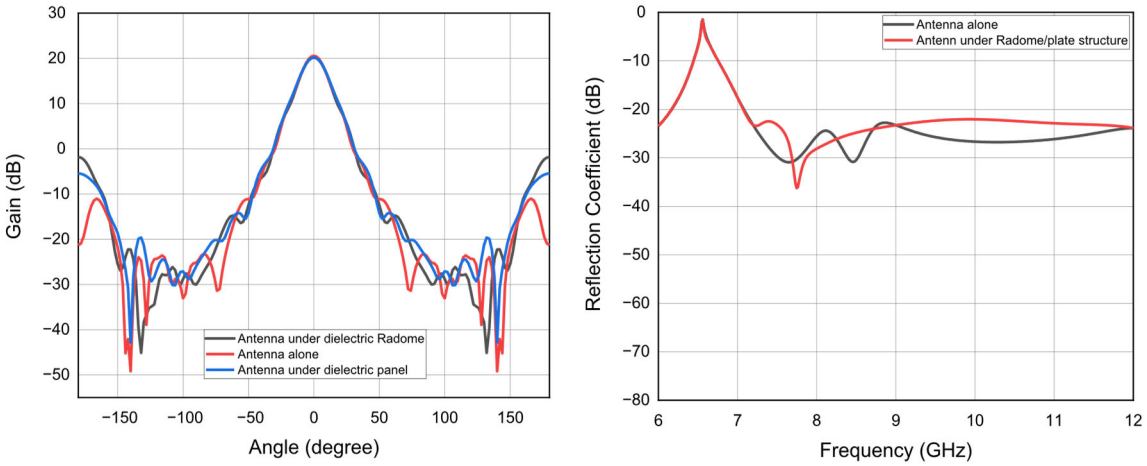

(**a**) (**b**)

Figure 15. *Cont.*

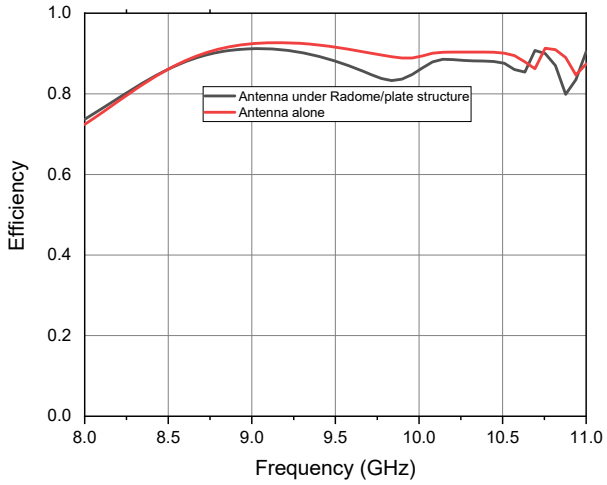

(**c**)

Figure 15. Various performance parameters for X-band horn antenna with and without dielectric cover: (**a**) antenna radiation patterns, (**b**) antenna S_{11} parameter to show impedance bandwidth and (**c**) radiation efficiency (radiated power).

3.3. EM Analysis of Millimeter-Wave Antenna

A substrate-integrated H-plane printed-horn antenna is simulated at 28 GHz under both dielectric structures as shown in Figure 16a,b. It is a low-profile novel structure antenna that gives a large continuous bandwidth in the millimeter-wave frequency range. The antenna alone gives 8.8 dBi of simulated gain with a 20 to 45 GHz large impedance bandwidth. It can be observed from Figure 17a that the antenna exhibits a total of 8.75 and 8.70 dBi in simulated gain under the dielectric panel and radome, respectively. This result confirms the optimal transparency properties of the dielectric structures even at frequencies higher than 20 GHz. Furthermore, a reflection coefficient and radiation efficiency graph are shown in Figure 17b,c. A small variable reflection is observed throughout the frequency sweep but a minimal reflection is observed at the resonance/design frequency.

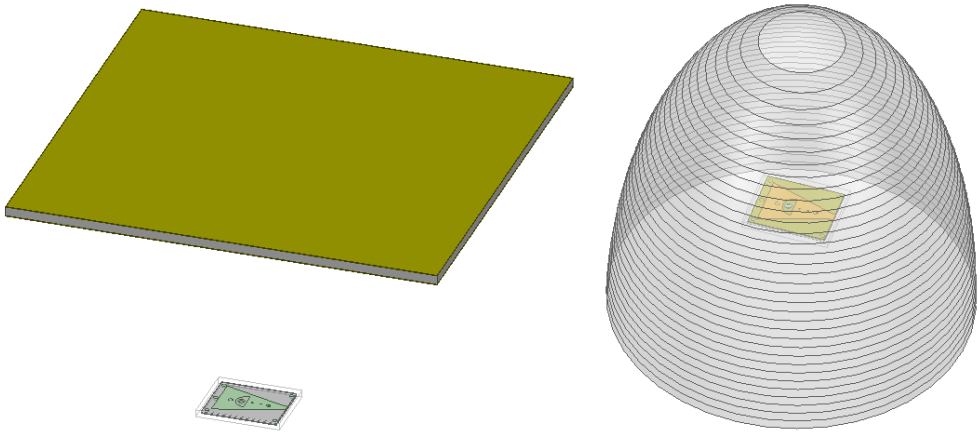

(**a**) (**b**)

Figure 16. A millimeter-wave antenna under dielectric-layered protective structures: (**a**) antenna under a dielectric-layered straight panel structure and (**b**) antenna under a dielectric-layered radome structure (bottom radius = 160 mm, middle layer radius = 140 mm and top layer radius = 36 mm).

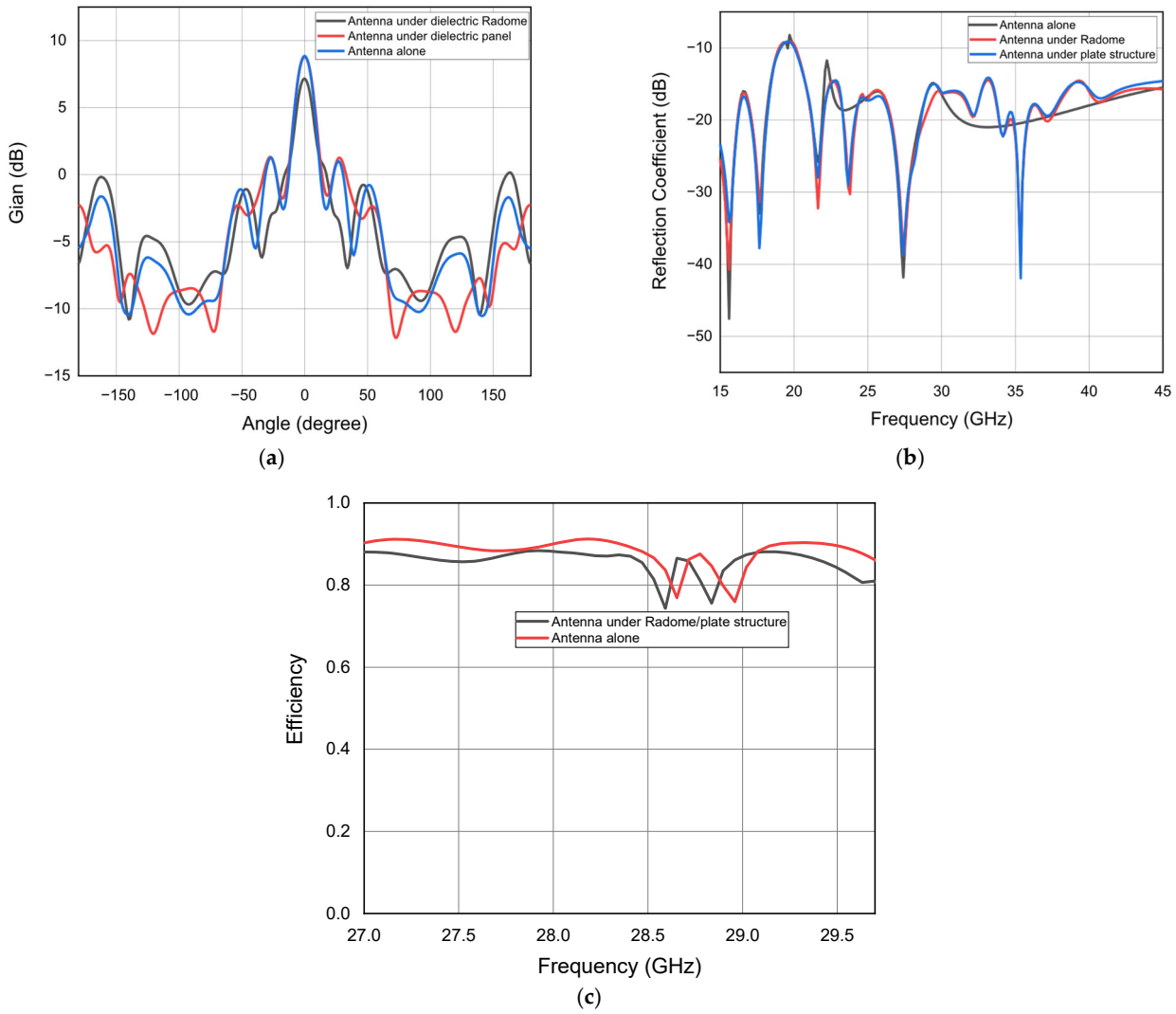

Figure 17. Various performance parameters for an mm-wave antenna with and without dielectric cover: (**a**) antenna radiation patterns, (**b**) antenna S_{11} parameter to show impedance band width and (**c**) efficiency.

In this antenna, the topologies of both directional and broadband antennas were used in a single antenna (horn-patch and micro-strip antenna). So, the directional gain antenna is giving very low reflections once again.

There is no effect found on HPBW (half-power beamwidth) for all three antenna cases during the electromagnetic analysis.

4. Fabrication and Measurements

In the first step, the prototypes of dielectric-layered radomes and plate structures along with different microwave and millimeter-wave antennas are realized and shown in Figure 18. In particular, the dome structure of the proposed dielectric radome (Figure 18a) is mostly used for airborne applications while the plate structure (Figure 18b) is favorable for ground applications mostly. They both have been realized and tested. The different antennas have been placed under these dielectric structures to measure radiation patterns. Moreover, Figure 18a shows the measurement set-up, where the profile dielectric structure is fixed along with an X-band profile antenna as the receiver antenna system. The reference antenna system of the anechoic chamber is used to check/test the profile receiver antenna

system. So, the gain pattern of the profile antenna system that is under a profile dielectric cover is measured. All antennas are tested in the same way.

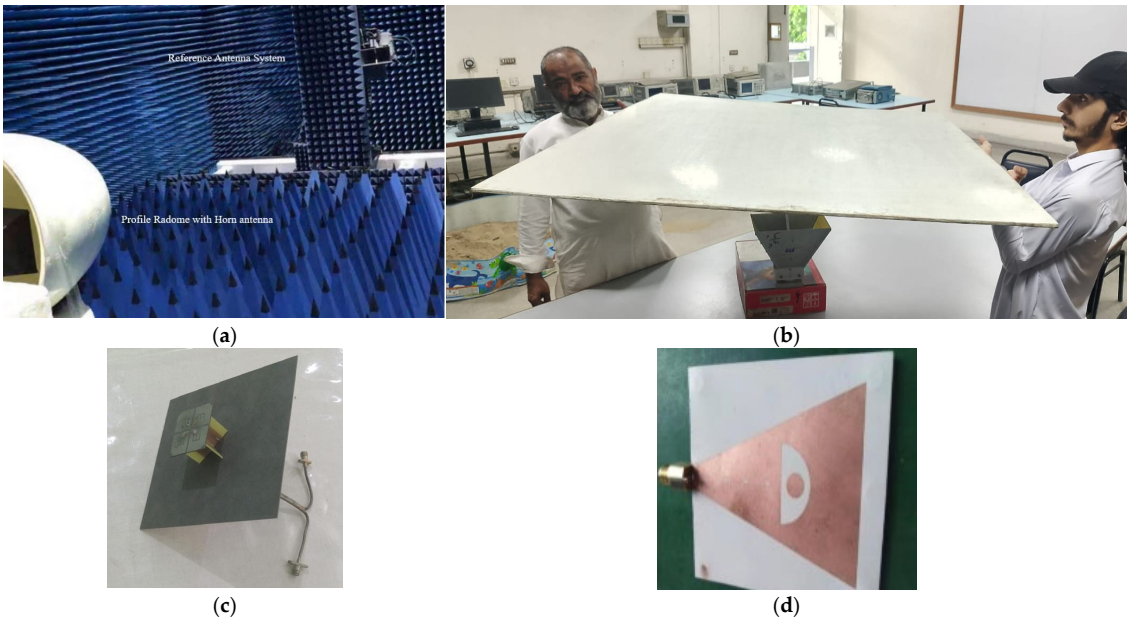

(**a**) (**b**)

(**c**) (**d**)

Figure 18. Fabricated antennas and dielectric structures: (**a**) X-band horn antenna under dielectric radome [8], (**b**) straight-plate A-sandwich dielectric structure, (**c**) sub-6 GHz 5G antenna and (**d**) millimeter-wave antenna [15].

In the first step, a fabricated sub-6 GHz 5G antenna has been characterized with and without a dielectric cover. It has been shown in Figure 19 that the radiation pattern has the same HPBW and is uniform. There is a minimal difference in the peak gain value. The measured antenna gain is 6.6 with and without dielectric structures. In the second step, a fabricated X-band horn antenna is tested at 9.4 GHz. It is clear from Figure 20 that no visible reflection has been observed for this directional antenna in the peak gain value, as expected from the simulation analysis. A little shift and value can be observed for the side lobe and back lobe of the antenna pattern. Minor differences and shifts have been observed solely due to the terminal resistance or fabrication effect. The antenna have a measured gain of 19.9 dBi.

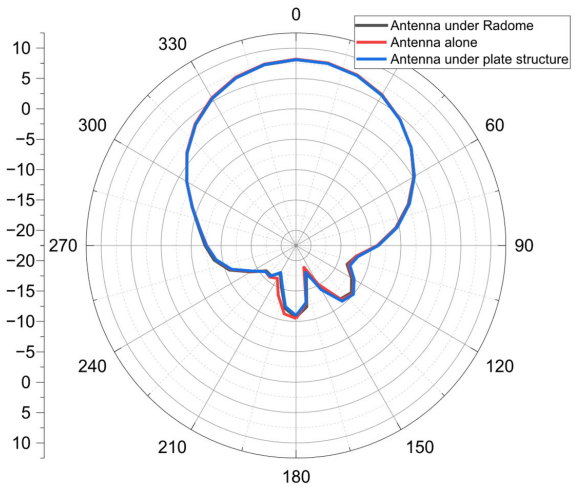

Figure 19. Measured 5G antenna patterns at 3.6 GHz.

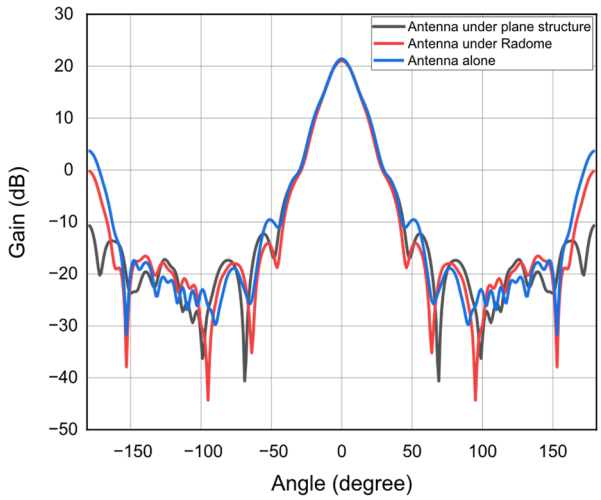

Figure 20. Measured horn-antenna patterns at 9.4 GHz with and without dielectric structures.

In the final step, a fabricated H-plane directional millimeter-wave antenna is tested under the prototype of the dielectric-layered structures, and the results have been measured. This is a substrate-integrated H-plane printed horn-patch directive antenna. In this case, the radiation pattern in Figure 21 shows a small difference in the peak gain value and a small upward shift in the side lobes and back lobe caused by the dielectric surface of the structures. The measured gain of the fabricated antenna under the dielectric plate structure and antenna alone is 8.67 dBi, while it further decreases to 8.64 dBi for the plate structure.

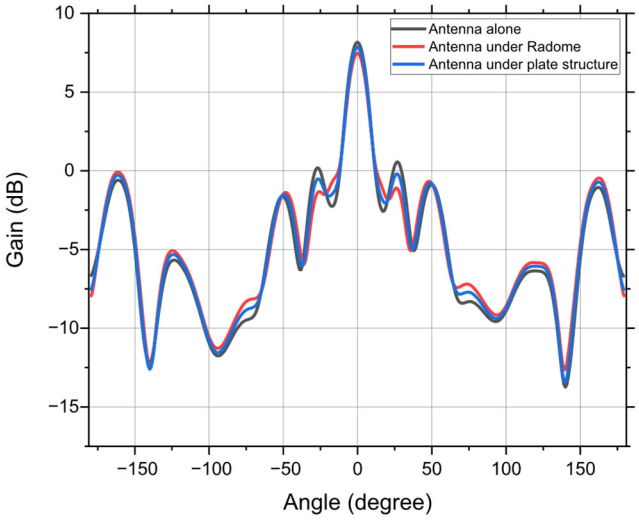

Figure 21. Millimeter-wave antenna patterns at 28 GHz with and without radome.

A comparison with the most related state-of-the-artworks [7–9,16,17] has been given in Table 1. It has been observed that a dielectric radome has been proposed in the mentioned papers (in Table 1) with various sandwich configurations (A-sandwich, C-sandwich and multi-layered sandwich) for a specified small range of frequencies within a specified band with insertion loss. The proposed dielectric structure covers a large frequency range with a minimal insertion loss where various small- or large-band antennas can be operated in the microwave and millimeter-wave range under the same dielectric structure. The ability to give minimal insertion losses for all the operational antennas (lying in the range 1–28 GHz) for any specified band makes this dielectric structure profile a good candidate for transceiver chimneys and towers. Moreover, this type of dielectric sheet (radome or a flat structure, depending upon the required application) not only provides external

protection to antenna installations but is also valuable for various electronic circuits and devices/machines like in [18,19].

Table 1. Comparison with related works.

No.	Ref.	Frequency	Insertion Loss
1	[7]	10 GHz	0.5–0.62 dB
2	[8]	9.4–16 GHz	0.1–0.3 dB
3	[9]	1.53–1.6 6.49–6.75 GHz	1.6 dB
4	[16]	NA	0.75–0.93 dB
5	[17]	8.5–10.3 GHz	0.3–0.6 dB
6	This work	1–28 GHz	0.03 dB

NA (not available).

The three tests demonstrate that the proposed dielectric-layered structure is electromagnetically transparent for a wide range of frequencies.

5. Conclusions

This work presents a unique design and evaluation of a dielectric-layered structure for antenna protection. The proposed structure operates over an extremely wide bandwidth and the experimental results demonstrate its minimal electromagnetic impact on the antenna patterns in microwave and millimeter-wave frequencies. This characteristic makes it a nearly universal protective solution for transceiver chimneys and towers. By providing consistent performance across a broad frequency range, the proposed dielectric structure offers great flexibility and versatility in antenna applications. Moreover, a dielectric thickness-specific operation coupled with a target angular line of sight (LOS) (e.g., for military applications of directional communications aims) may enable an angular-specific transmission capability, avoiding the standard 360° communication operation. Future research could explore further optimization and customization of the structure to accommodate specific antenna designs and operational requirements.

Author Contributions: H.U.T.: Writing—original draft, Methodology, Investigation, Simulations and Electromagnetic analysis; L.F.: —Conceptualization, Formal analysis, Data curation and Supervision; S.S.I.H.: —Fabrication and Measurement; L.C.: —Review—editing and Validation. All authors have read and agreed to the published version of the manuscript.

Funding: This research received no external funding.

Data Availability Statement: The original contributions presented in this study are included in the article. Further inquiries can be directed to the corresponding author.

Acknowledgments: We express our gratitude to Chiara De Pascali at IMM-CNR Lecce, Italy for participating in the revision stage for upgrading the paper by doing additional simulations and analysis.

Conflicts of Interest: The authors declare no conflicts of interest.

References

1. Yurchenko, V.B.; Altintas, A.; Nosich, A.I. Numerical optimization of a cylindrical reflector-in-radome antenna system. *IEEE Trans. Antennas Propag.* **1999**, *47*, 668–673. [CrossRef]
2. Nair, R.; Vandana, S.; Sandhya, S.; Jha, R.M. Temperature-dependent electromagnetic performance predictions of a hypersonic streamlined radome. *Prog. Electromagn. Res.* **2015**, *154*, 65–78. [CrossRef]
3. Chen, F.; Shen, Q.; Zhang, L. Electromagnetic optimal design and preparation of broadband ceramic radome material with graded porous structure. *Prog. Electromagn. Res.* **2010**, *105*, 445–461. [CrossRef]
4. Pei, Y.; Zeng, A.; Zhou, L.; Zhang, R.; Xu, K. Electromagnetic optimal design for dual-band radome wall with alternating layers of staggered composite and Kagome lattice structure. *Prog. Electromagn. Res.* **2012**, *122*, 437–452. [CrossRef]

5. Nair, R.U.; Jha, R.M. Novel A-sandwich radome design for airborne applications. *Electron. Lett.* **2007**, *43*, 787–788. [CrossRef]
6. Nair, R.U.; Jha, R.M. Electromagnetic performance analysis of a novel monolithic radome for airborne applications. *IEEE Trans. Antennas Propag.* **2009**, *57*, 3664–3668. [CrossRef]
7. Yazeen, P.M.; Vinisha, C.V.; Vandana, S.; Suprava, M.; Nair, R.U. Electromagnetic performance analysis of graded dielectric inhomogeneous streamlined airborne radome. *IEEE Trans. Antennas Propag.* **2017**, *65*, 2718–2723. [CrossRef]
8. Tahseen, H.U.; Yang, L.; Zhou, X. Design of FSS-antenna-radome system for airborne and ground applications. *IET Commun.* **2021**, *15*, 1691–1699. [CrossRef]
9. Zhou, L.; Pei, Y.; Fang, D. Dual-band A-sandwich radome design for airborne applications. *IEEE Antennas Wirel. Propag. Lett.* **2015**, *15*, 218–221. [CrossRef]
10. Nair, R.U.; Jha, R.M. Electromagnetic design and performance analysis of airborne radomes: Trends and perspectives. *IEEE Antennas Propag. Mag.* **2014**, *56*, 276–298. [CrossRef]
11. Ismail, Ç.O.R.; Birsen, S. Geni¸s bantlı radom analizi ve eniyilenmesi analysis and optimization of wideband radomes. In Proceedings of the 26th Signal Processing and Communications Applications Conference, Izmir, Turkey, 2–5 May 2018.
12. Xu, W.; Duan, B.Y.; Li, P.; Hu, N.; Qiu, Y. Multiobjective particle swarm optimization of boresight error and transmission loss for airborne radomes. *IEEE Trans. Antennas Propag.* **2014**, *62*, 5880–5885. [CrossRef]
13. Nair, R.U.; Suprava, M.; Jha, R.M. Graded dielectric inhomogeneous streamlined radome for airborne application. *Electron. Lett.* **2015**, *51*, 862–863. [CrossRef]
14. Rudge, A.W. (Ed.) Radomes. In *The Handbook of Antenna Design*; IET: London, UK, 1982; Volume 2.
15. Tahseen, H.U.; Yang, L.; Hongjin, W. A Broadband H-plane Printed Horn Antenna with Sandwich Substrate Structure for Millimeter-wave Applications. *Appl. Comput. Electromagn. Soc. J. (ACES)* **2021**, *36*, 295–301. [CrossRef]
16. Xu, W.; Duan, B.Y.; Li, P.; Qiu, Y. Study on the Electromagnetic Performance of Inhomogeneous Radomes for Airborne Applications—Part II: The Overall Comparison with Variable Thickness Radomes. *IEEE Trans. Antennas Propag.* **2017**, *65*, 3175–3183. [CrossRef]
17. Narayan, S.; Gulati, G.; Sangeetha, B.; Nair, R.U. Novel Metamaterial-Element-Based FSS for Airborne Radome Applications. *IEEE Trans. Antennas Propag.* **2018**, *66*, 4695–4707. [CrossRef]
18. Merenda, M.; Iero, D.; G. Della Corte, F. CMOS RF Transmitters with On-Chip Antenna for Passive RFID and IoT Nodes. *Electronics* **2019**, *8*, 1448. [CrossRef]
19. Merenda, M.; Felini, C.; Della Corte, F.G. A Monolithic Multisensor Microchip with Complete On-Chip RF Front-End. *Sensors* **2018**, *18*, 110. [CrossRef] [PubMed]